Slip distribution and stress changes associated with the 1999 November 12, Düzce (Turkey) earthquake ($M_w = 7.1$)

Murat Utkucu,[1] Süleyman S. Nalbant,[2] John McCloskey,[2] Sandy Steacy[2] and Ömer Alptekin[1]

[1] *İstanbul University, Department of Geophysics, 34850 Avcılar, İstanbul, Turkey*
[2] *Geophysics Research Group, School of Biological & Environmental Sciences, The University of Ulster, Coleraine, UK. E-mail: ss.nalbant@ulster.ac.uk*

SUMMARY

The 1999 November 12 Düzce earthquake ($M_w = 7.1$) was apparently the eastward extension of the August 17, İzmit earthquake ($M_w = 7.4$). The Düzce event caused heavy damage and fatalities in the cities of Düzce and Bolu. Here a finite-fault inversion method with five discrete time windows is applied to derive the co-seismic slip distribution of the Düzce earthquake. The fault plane is best modelled as a 40×20 km^2 plane, with a strike of $262°$ and a dip of $65°$ to the north, and that the majority of slip occurred in two distinct patches on either side of the hypocentre, implying bilateral rupture. The possible triggering of this event by the İzmit earthquake is investigated using Coulomb stress modelling of all large events since 1943 with the inclusion of secular loading. The results show that although the Düzce rupture plane was in a stress shadow prior to the İzmit earthquake, that event caused a significant Coulomb stress load, taking the Düzce fault out of the stress shadow, which probably precipitated failure. A comparison of the mapped Coulomb stress change with the inferred slip shows no correlation between the two. Finally, the stress modelling indicates that the northern branch of the North Anatolian fault zone, beneath the Sea of Marmara towards the city of İstanbul, is presently the most highly loaded segment of the North Anatolian Fault Zone.

Key words: coseismic slip distribution, Coulomb stress change, the 1999 Düzce earthquake.

INTRODUCTION

Approximately, 3 months after the devastating 1999 August 17, İzmit earthquake ($M_w = 7.4$), an earthquake with magnitude $M_w = 7.1$ occurred in northwest Turkey on 1999 November 12, causing heavy damage and fatalities in the cities of Düzce and Bolu (Fig. 1). As its surface rupture initiated south of Gölyaka, near the surface rupture termination of the İzmit earthquake, and proceeded to the east, it appears to be an eastward extension of the İzmit rupture (Figs 1 and 2). The occurrence of the November 12 Düzce earthquake was not surprising since the August 17, İzmit earthquake had increased the Coulomb stress to the east of the ruptured area (Hubert-Ferrari *et al.* 2000). The İzmit and the Düzce earthquakes created havoc and caused severe destruction not only in northwestern Turkey but throughout the country because the region has a dense population, houses the main industrial facilities, and because major transportation lines that connect Turkey to Europe cross the region.

The general tectonic configuration of Anatolia and surrounding areas can be explained as a collision of the Arabian and African plates with the Eurasian and Anatolian plates (Fig. 3). Compressed between approximately northward-moving Arabian and relatively stable Eurasian plates, the Anatolian plate is forced to escape west-

ward and this movement changes direction to the southwest in West Anatolia and the South Aegean Sea, causing counter-clockwise rotation of the Anatolian plate (McKenzie 1972; Jackson & McKenzie 1984; McClusky *et al.* 2000). The westward movement of the Anatolian plate is accommodated by the right lateral North Anatolian Fault Zone (NAFZ) and the left-lateral East Anatolian Fault Zones (EAFZ). GPS studies indicate a slip rate of 24 ± 1 and 9 ± 1 mm yr^{-1} for the NAFZ and the EAFZ, respectively (McClusky *et al.* 2000).

The Düzce earthquake, as with the 3 month earlier İzmit earthquake, occurred on the NAFZ, which extends in a roughly EW direction from the Karlıova triple junction in the east to the northern Aegean Sea in the west (Fig. 3). The geometry and segmentation of the fault zone were studied in detail by Barka & Kandisky-Cade (1988). Source mechanisms of the earthquakes along the fault zone show mostly right-lateral strike-slip faulting (McKenzie 1972; Jackson & McKenzie 1984) and complex rupture processes (Pınar *et al.* 1994, 1996). Between 1939 and 1967, the fault zone experienced six strike-slip earthquakes with magnitude $M > 7$ migrating toward the west (Toksöz *et al.* 1979; Barka 1996) in a sequence consistent with successive Coulomb stress triggering (Stein *et al.* 1997). The August 17 İzmit earthquake was the final one of this sequence and drew the attention of several researchers (Barka 1999;
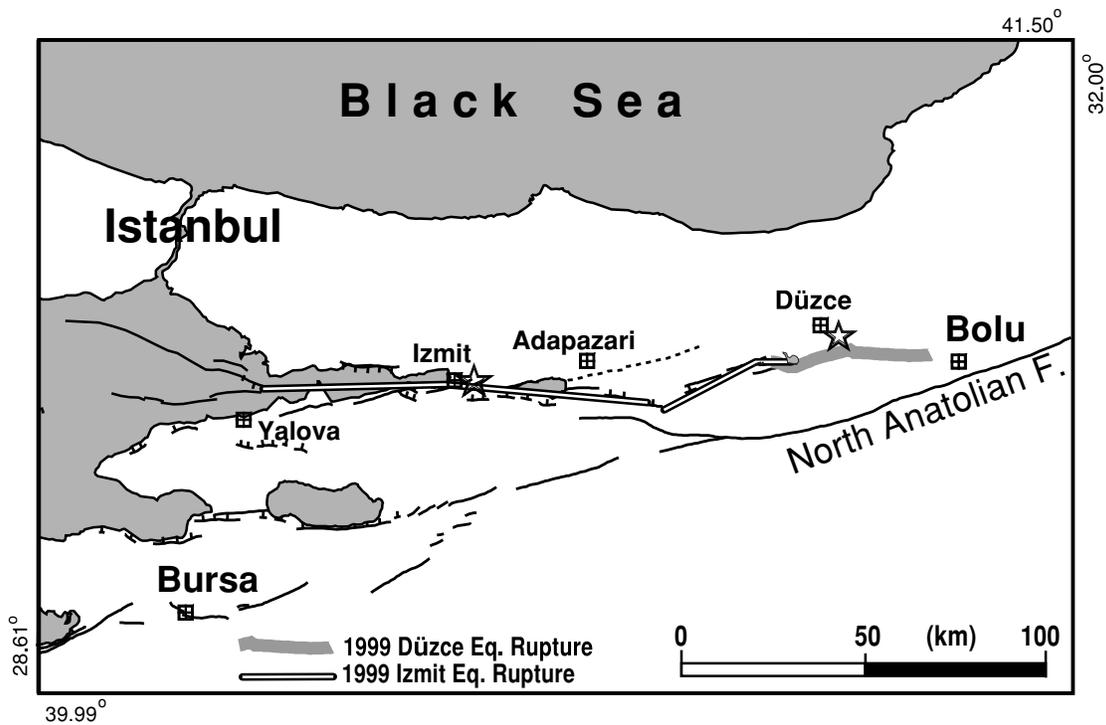
Figure 1. Fault map of east Marmara region showing the epicentres (stars) of the 1999 İzmit and Düzce earthquakes. The İzmit earthquake rupture zone is modified from Delouis *et al.* (2002). Some major cities that were affected by the earthquakes are also marked.
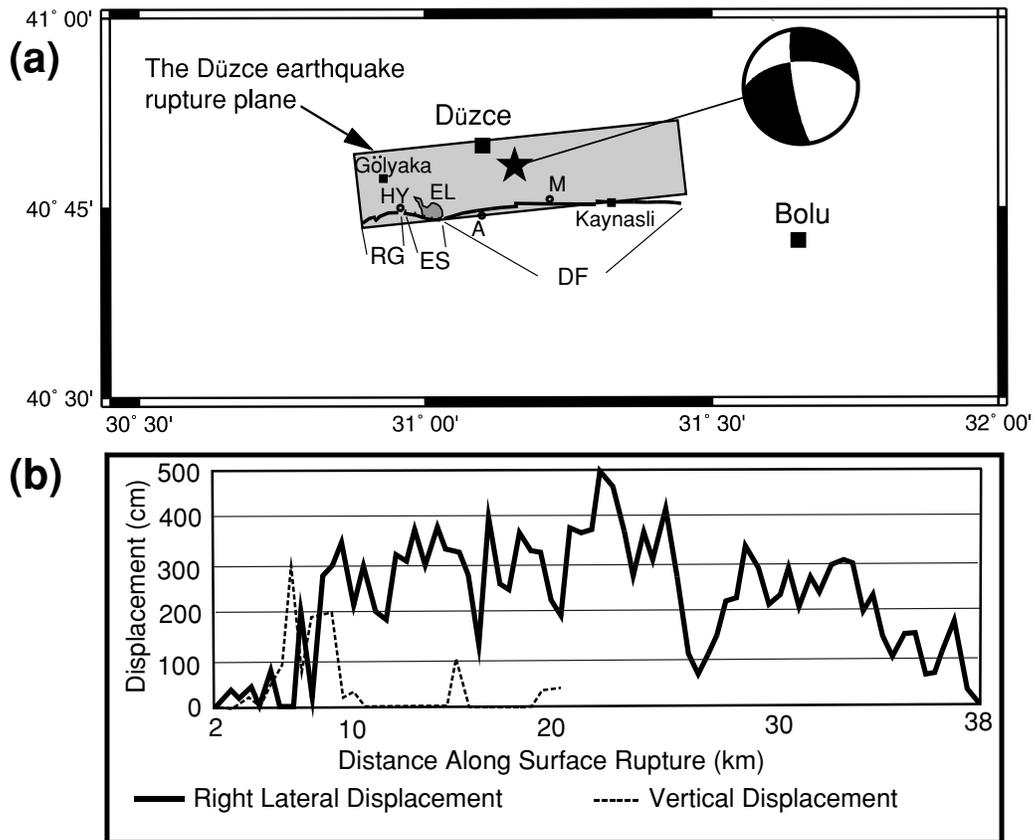

Figure 2. Location map showing mapped surface rupture of the Düzce earthquake (a) and surface slip distribution along the strike (b) (adapted from Barka *et al.* 1999 and Akyüz *et al.* 2002). The earthquake epicentre (solid star), surface projection of the model fault used in the study (large rectangle), and the focal mechanism solution are also shown (a). RG and ES are the ruptured part of the Gölyaka fault segment during the İzmit earthquake, the Eften lake step over, and the Düzce fault, respectively. Abbreviated town names along the rupture are Haci Yakup (HY), Aydinpinar (A) and Mengencik (M). EL stands for Eften Lake.
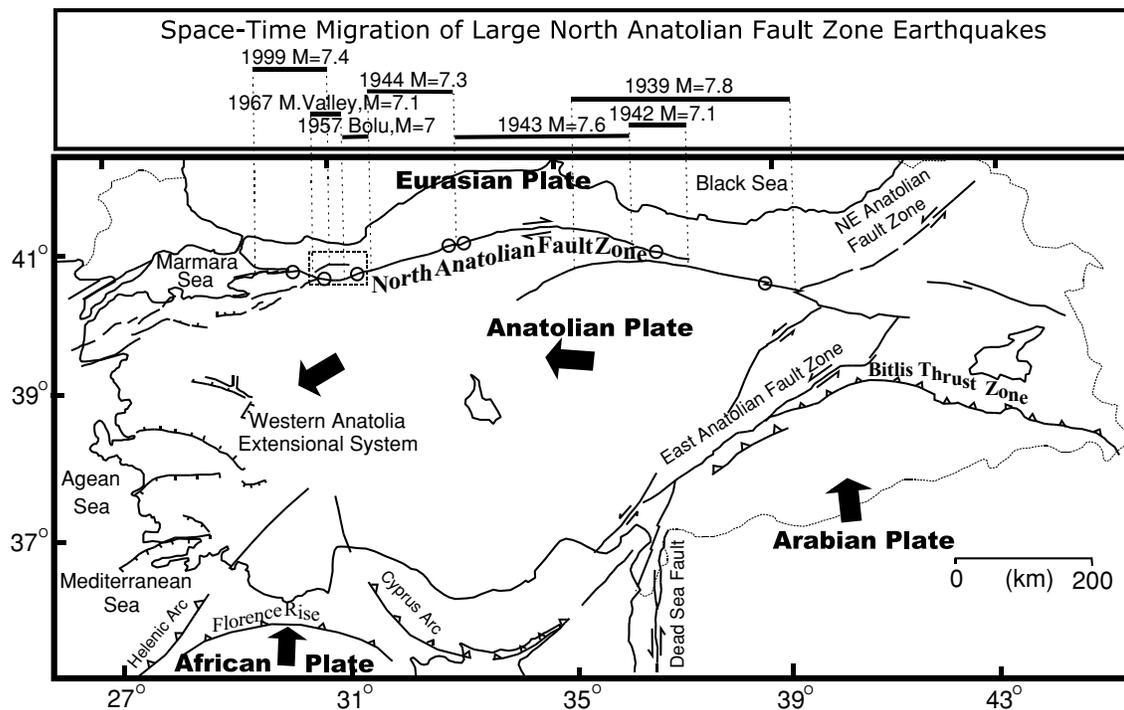
Figure 3. Map showing major tectonic elements of Turkey and space–time migration of the seven large earthquakes along North Anatolian Fault Zone, the period between 1939 and 1999 (compiled from Barka & Kandisky-Cade 1988; Barka 1996). The dashed rectangle indicates the map area shown in Fig. 2 and large arrows represent the direction of relative plate motions.

Toksöz *et al.* 1999; Parsons *et al.* 2000; Delouis *et al.* 2002; Tibi *et al.* 2001; Pınar *et al.* 2001; Honkura *et al.* 2000). Coulomb stress changes resulting from the 1999 İzmit earthquake were modelled by Hubert-Ferrari *et al.* (2000). Their study indicates that the İzmit event strongly loaded the fault segments extending under the Marmara Sea and the fault segment that ruptured during the Düzce earthquake.

The NAFZ bifurcates into two strands near the Bolu province (Barka 1996), and the Düzce fault segment along with the Gölyaka fault segment constitute the northern strands (Fig. 2). The southern strand had ruptured during the 1957 Bolu and 1967 Mudurnu Valley earthquakes but the northern strand did not rupture until 1999 (Figs 1 and 3). Therefore, Barka (1996) indicated the possibility of the Düzce fault segment producing a large earthquake; this oc-

curred with the 1999 November 12 earthquake ($M_S = 7.2$) that ruptured the Düzce fault. The epicentre of the earthquake was located at (40.818°N, 31.198°E) by the SABONET network of the Earthquake Research Department (ERD) of Turkey. Focal mechanism solutions of the earthquake show predominantly right lateral strike-slip faulting with a small normal faulting component on a roughly east–west-striking northerly dipping fault plane consistent with the observed surface rupture (Tibi *et al.* 2001, Harvard CMT). The source parameters are summarized at Table 1. The mainshock was followed by abundant aftershock activity including several $M \geq 5.0$ events. Regional moment tensor inversions of the majority of the large aftershocks show right lateral source mechanisms and define an EW-striking northerly dipping fault plane (Örgülü & Aktar 2001).

Table 1. Source parameters of the 1999 November 12, Düzce earthquake. The strike/dip/rake convention of Aki & Richards (1980) is used.

	ERD	USGS	HRV	Tibi *et al.* (2001)[1]	Pınar *et al.* (2001)[2]	Ayhan *et al.* (2001)[3]	Wright *et al.* (2001)[4]
Latitude (deg)	40.818	40.77	40.93				
Longitude (deg)	31.198	31.15	31.25				
Depth (km)	12.5	14	18				
$M_o(\times 10^{19}$ N m)		4.5	6.7	4.6		5.1–5.8	4.2 ± 0.4
M_w		7.1	7.2				
Strike (deg)			264	264	262		
Dip (deg)			54	64	65		57 ± 4
Rake (deg)			−167	184	−178		−134 ± 17

[1] From the inversion of the *P* and *SH* waveforms.
[2] From the inversion of the *P* and *SH* waveforms.
[3] From the inversion of the GPS data.
[4] From the inversion of the InSAR data.

The surface ruptures extend from south of Gölyaka to the east of Kaynaşli town with a total rupture length of approximately 40 km (Fig. 2) (Akyüz *et al.* 2002). The location of the epicentre relative to the extension of the surface rupture implies bilateral rupturing (Fig. 2). To the west of the surface rupture, the earthquake ruptured the east extreme of the Gölyaka fault segment, which had already been ruptured by the İzmit event, for a length of 9 km (Figs 1 and 2). The rupture steps over the Düzce fault segment after crossing the Eften lake pull-apart basin to the south of the Eften lake, where maximum vertical offset (as much as 3 m) was observed along the surface rupture (Barka *et al.* 1999) (Fig. 2). Along the Düzce fault, where the maximum displacement during the earthquake was observed, surface faulting is nearly pure right lateral and consists of three left-stepping subsegments. Maximum right lateral displacement reached 4.5 m to the south of the Mengencik village (Barka *et al.* 1999) (Fig. 2). The surface rupture then crosses the centre of Kaynaşli town and terminates approximately 5 km east of it. Maximum right-lateral offset between Kaynaşli town and the east extreme of the surface rupture was approximately 1.5 m (Barka *et al.* 1999).

The aims of this study are to find a finite-fault slip distribution model for the Düzce earthquake from the inversion of the far-field *P* and *SH* waveforms and to investigate the stress loading of the 1999 İzmit earthquake on the Düzce fault and the stress condition of the NAFZ after the 1999 İzmit and Düzce earthquakes.

FINITE-FAULT MODELLING

The method of finite-fault waveform inversion employed in the study was originally developed by Hartzell & Heaton (1983) and has been applied to many earthquakes to obtain their rupture characteristics (e.g. Wald & Heaton 1994; Mendoza 1995; Langer & Hartzell 1996). A detailed explanation of the method is given by Hartzell & Heaton (1983) and Wald & Heaton (1994) and will only be briefly discussed here. We use 16 teleseismic broad-band *P* and eight teleseismic long-period *SH* waveforms recorded by the Global Digital Seismograph Network (GDSN) to infer the finite fault slip model of the Düzce earthquake. Only the stations having epicentral distances
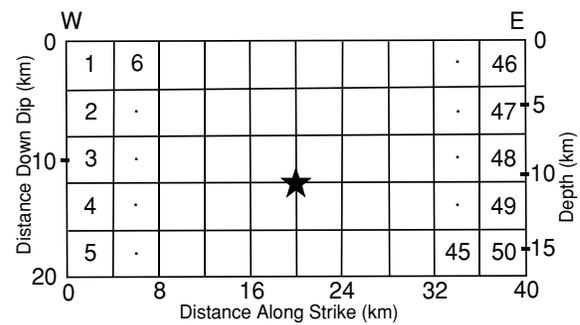
Figure 4. Fault model parametrization used to obtain the slip distribution of the Düzce earthquake. The fault model has a length of 40 km and a width of 20 km and is discretized as 50 square subfaults each with 4 km on a side. The solid star denotes the hypocentre.

between 30° and 95° for *P* waveforms and 40° and 85° for *SH* waveforms are used to avoid upper-mantle distortions and core–mantle boundary diffractions. After removing the instrument response, the *P* waveforms are resampled using a time step of 0.25 s and bandpass filtered from 0.01 to 1.0 Hz using a Butterworth filter. The *SH* waveform sampling interval is taken as 1 s and bandpass filtered from 0.01 to 0.5 Hz using the same bandpass filter. Teleseismic velocity recordings are used in the inversion. Teleseismic stations included in the inversion are tabulated in Table 2. The first 30 s of the *P* waveforms are modelled in the study. This record length is chosen from the fault plane dimensions and rupture velocity used in the modelling.

In the model, the Düzce rupture is represented by a fault plane with dimension of 40×20 km^2, which is divided into 50 square subfaults (Fig. 4). The dimension of the fault plane is based on previous studies (e.g. Ayhan *et al.* 2001; Tibi *et al.* 2001; Bürgmann *et al.* 2002) and the surface rupture associated with the earthquake. The strike and dip of the fault plane were determined very precisely by the previous source studies (Table 1) and fixed at 262° and 65°, respectively. Rake is allowed to vary between −180° and −90° for each subfault. The fault plane is then placed in the velocity structure shown in Table 3, extending from the surface to a depth of 18.126 km. Epicentre

Table 2. Teleseismic stations that are used in the study.

Station	Latitude (deg)	Longitude (deg)	Distance (deg)	Azimuth (deg)	Phase
MA2	59.340	150.460	68.00	28.36	*P, SH*
YAK	62.020	129.720	58.36	33.03	*P, SH*
TATO	24.975	121.488	74.18	70.41	*P*
AAK	42.639	74.494	32.01	72.13	*P*
ENH	30.271	109.487	62.48	72.48	*P*
BDFB	−15.641	−48.014	92.28	251.21	*P*
CMLA	37.763	−25.524	43.23	285.22	*P*
SJG	18.111	−66.150	83.62	288.46	*P*
DWPF	28.112	−81.432	87.07	305.39	*P*
SSPA	40.640	−77.891	76.24	312.41	*P*
HKT	29.961	−95.838	93.93	316.10	*P*
CCM	38.055	−91.244	85.22	318.18	*P, SH*
SFJ	66.996	−50.615	49.93	329.64	*P*
FFC	54.724	−101.977	76.42	334.34	*P*
DAV	7.087	125.574	88.66	81.78	*P*
CHTO	18.790	98.976	61.21	89.37	*P*
TIXI	71.629	128.869	54.01	22.71	*SH*
WMQ	43.821	87.695	41.11	66.27	*SH*
SUR	−32.379	20.811	73.77	189.08	*SH*
ASCN	−7.932	−14.360	64.18	231.78	*SH*
BINY	42.199	−75.986	74.14	312.61	*SH*

Table 3. Velocity structure.

Thickness (km)	V_P (km s^{-1})	V_S (km s^{-1})	ρ (kg m^3)
5	4.60	3.00	2660
16	5.80	3.29	2750
20	7.00	3.89	2880
–	8.10	4.44	3300

Table 4. Inversion results for different rupture velocities.

Rupture velocity (km s^{-1})	Euclidean norm
2.3	12.163
2.5	12.066
2.7	12.106
2.9	12.121

coordinates determined by the SABONET network of the Earthquake Research Department of Turkey (40.818°N, 31.198°E) are used as the rupture initiation point that corresponds to a hypocentral depth of 10.7 km on the model fault plane (Fig. 4). Generalized ray theory (Langston & Helmberger 1975) is used for computation of point source responses. The crustal velocity structure used for computation of point sources is based on the study of Kenar & Toksöz (1989) (Table 3). After appropriate lags in time to represent propagation of rupture across each subfault and to accommodate traveltime differences between each source–station pair, the point source responses are then summed to construct subfault synthetic seismograms (Green's functions) for each station included in the inversion. Attenuation is incorporated by convolving subfault synthetics with a constant attenuation operator, t^* of 0.7 s for P and 4 s for SH waves. The subfault synthetics are bandpass filtered for the same frequency range, differentiated to ground velocities and sampled for the same time interval as the observations.

Rupture velocity and source rise time are also required for generating the synthetics. Following Hartzell & Heaton (1983), flexibility in rupture velocity has been allowed by introducing time window parametrization to accommodate complexity arising from multiple shock events and locally variable rupture velocities and, in turn, to obtain a more accurate slip distribution. The time window approach allows fault slip with smaller rupture velocities than a maximum rupture velocity specified for the calculation of the synthetics in the inversion. Tibi *et al.* (2001) estimated a rupture velocity of km s^{-1} for the earthquake. Therefore, starting with the rupture velocity of 2.7 km s^{-1}, which is 85 per cent of the shear velocity of the top two layers of the velocity model (Table 3), maximum rupture velocities of 2.3, 2.5, 2.7 and 2.9 km s^{-1} were tried in the inversion. Five time windows were used and the source rise time for each window was represented by an isosceles triangle with 0.4 s rise and fall. Each time window was delayed by 0.8 s from the previous one so that they did not overlap, allowing a total slip duration of 4 s for each subfault. The subfault synthetics and the observed data define an over-determined system of linear equations of the form $\mathbf{Ax} = \mathbf{b}$, where $\mathbf{x}$ is the solution vector including the slip weights to be given to each subfault so that the synthetics fit the observed data. The solution vector, $\mathbf{x}$, is solved using a Householder least-squares inversion method (Lawson & Hanson 1974) that constrains each value of the solution vector to be greater than or equal to zero. The inversion is further constrained by using smoothing and moment minimization constraints (Hartzell & Heaton 1983). These constraints allow the smoothest slip distribution model with minimum seismic moment to be obtained by the inversion.

FINITE-FAULT MODELLING RESULTS AND DISCUSSION

The slip distribution models resulting from the inversions with different maximum rupture velocities are very similar. The misfit between the synthetics and the data for these different inversions is defined as the Euclidean norm of the residual vector and is given in Table 4. The inversion with a rupture velocity of 2.5 km s^{-1} gives the smallest misfit error (Table 4) and it is therefore selected as the best-fitting slip model of the Düzce earthquake (Fig. 5). The strike-slip and dip-slip components (top and middle frame) of the coseismic slip along with their vector sum (bottom frame) are shown separately in Fig. 5. Observed teleseismic waveforms and the synthetic waveforms produced for the slip model are compared in Fig. 6. The slip model indicates two major slip regions or asperities. The source regions with slip amplitude higher than 200–250 cm are considered as asperities. Following this consideration the rupture areas of the LA and SA are approximated by a large rectangle and a small square, respectively, in Fig. 5. The largest asperity (LA) is located just updip and east of the hypocentre with a peak slip value of 596 cm. Its area extends west of the hypocentre for approximately 10 km resulting in an overall rupture area of approximately 20 × 10 km^2. The smaller asperity (SA) is located in the western shallow part of the fault with a peak slip amplitude of approximately 313 cm. The SA covers the depth above 5 km with a length of approximately 7 km in the western corner of the fault. There is also a tiny circular area of slip of as much as 2 m downdip of the SA. Although both the SA and the circular area of slip are quite small, numerous finite-fault studies (e.g. Hartzell & Heaton 1983; Hartzell 1989; Wald *et al.* 1991; Mendoza *et al.* 1994; Hartzell *et al.* 1999) have shown that slip patches of such sizes are clearly resolvable with teleseismic data. The overall pattern of the slip indicates that the rupture propagated bilaterally mainly updip from the hypocentre, initially breaking the LA and proceeding to break the SA.

As Fig. 5 indicates, the rupture was almost pure strike-slip. Normal slip occurred only west and updip of the hypocentre and is mostly below 100 cm. This can clearly be seen in Fig. 7, which shows the slip vectors for individual subfaults. Although the slip vectors define an average rake angle of −171° for the overall rupture, the largest slip vectors indicate almost pure right lateral slip. These rake angles do not differ from the rake values resulting from the previous seismic waveform inversion studies, all of which indicate almost pure right-lateral strike-slip (Table 1). There is, however, a significant difference between the rake angle obtained seismically and geodetically. In their multiple-segment modelling of the InSAR data, Wright *et al.* (2001) obtained a rake angle of −134°, which requires a significant component of dip-slip. However, in their single-fault modelling, they obtained a rake angle that is almost the same as derived from seismic waveform inversions −178°. They attribute these differences to the sensitivity of the InSAR data to vertical motion. The estimated seismic moment for our slip model is 5.5 × 10^{26} dyne cm, which corresponds to a moment magnitude of $M_w = 7.1$.

As mentioned above, the Düzce earthquake re-ruptured the western part of the Gölyaka segment (RG in Fig. 2) for 9 km, which had already been ruptured by the İzmit earthquake (Fig. 2). Possibly, the SA represents the continuation of the rupture of LA on this re-ruptured segment. The modelled slip gradually decreases and then vanishes approximately 6 km east of Kaynaşli town similar to the observed surface ruptures (Fig. 3) (Barka *et al.* 1999). The maximum surface displacements observed between Kaynaşli and Mengencik coincide well with the maximum slip region of the LA.
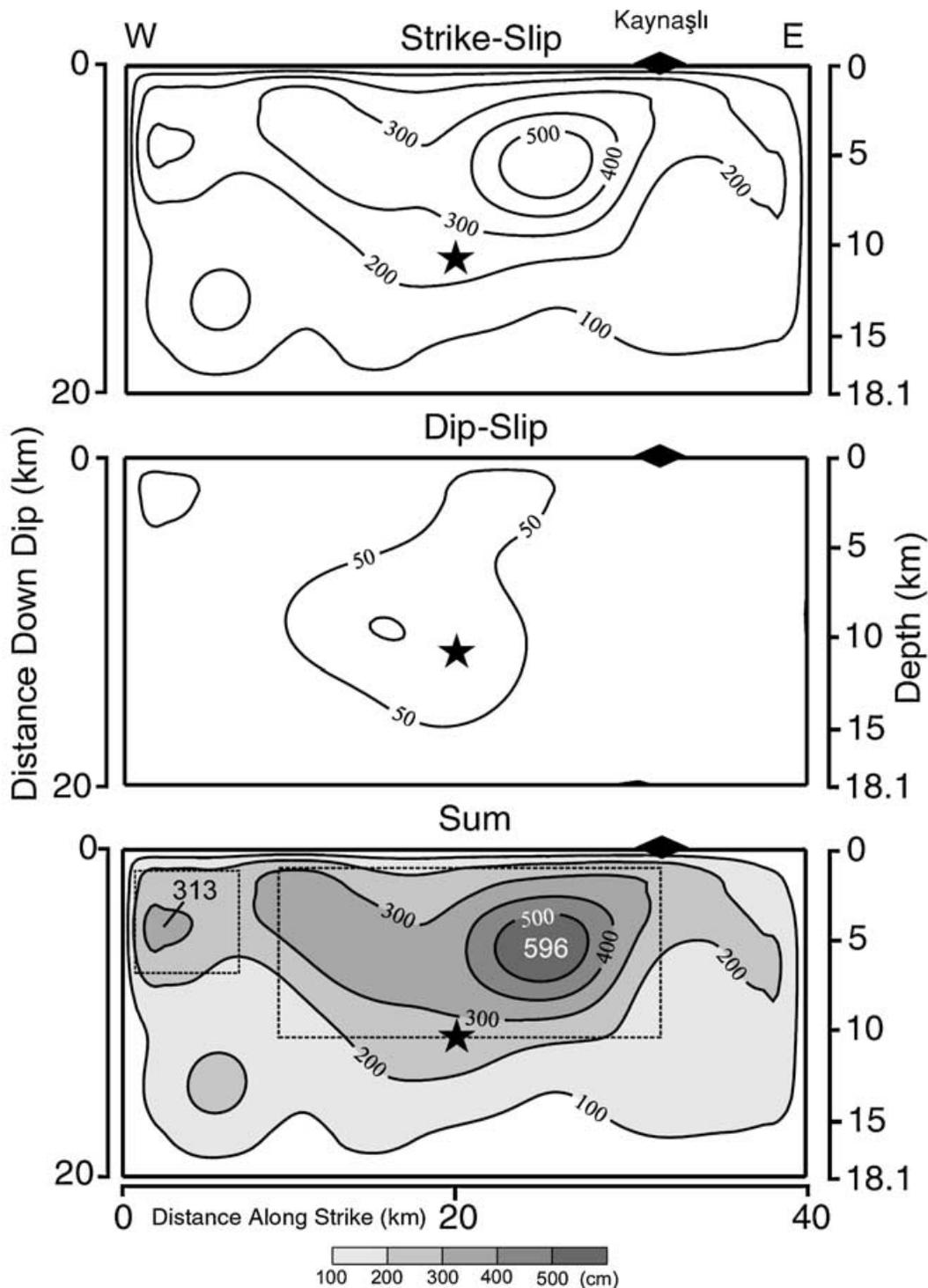
Figure 5. Contour map of coseismic displacements obtained for the Düzce earthquake in the study for strike-slip (top) and dip-slip (middle) components and their vector sum (bottom). Note that the slip is contoured at 50 cm intervals for the dip-slip motion while the strike-slip component and vector sum are contoured at 100 cm intervals. The solid star represents the hypocentre and the large and small squares enclose approximate rupture areas of the LA and SA, respectively.

The maximum surface displacement between Mengencik and Eften Lake ranging from 2 to 4 m also coincides well with the western extent of the slip area of the LA in the slip model. However, the slip model indicates over 2 m of slip for the westernmost part of the rupture while the observed surface rupture is smaller than 1 m, with only a local peak of approximately 2 m. In general, however, near-surface displacements as determined by the modelling are in

good agreement with the observed surface displacements, although no surface slip constraints were imposed in the inversion.

Since we used five time windows in our initial parametrization, the change of slip rise time across the fault plane can be determined by investigation of the individual slip contribution of each time window displayed in Fig. 8. The overall pattern of the slip indicates that the rupture propagated bilaterally mainly updip from the

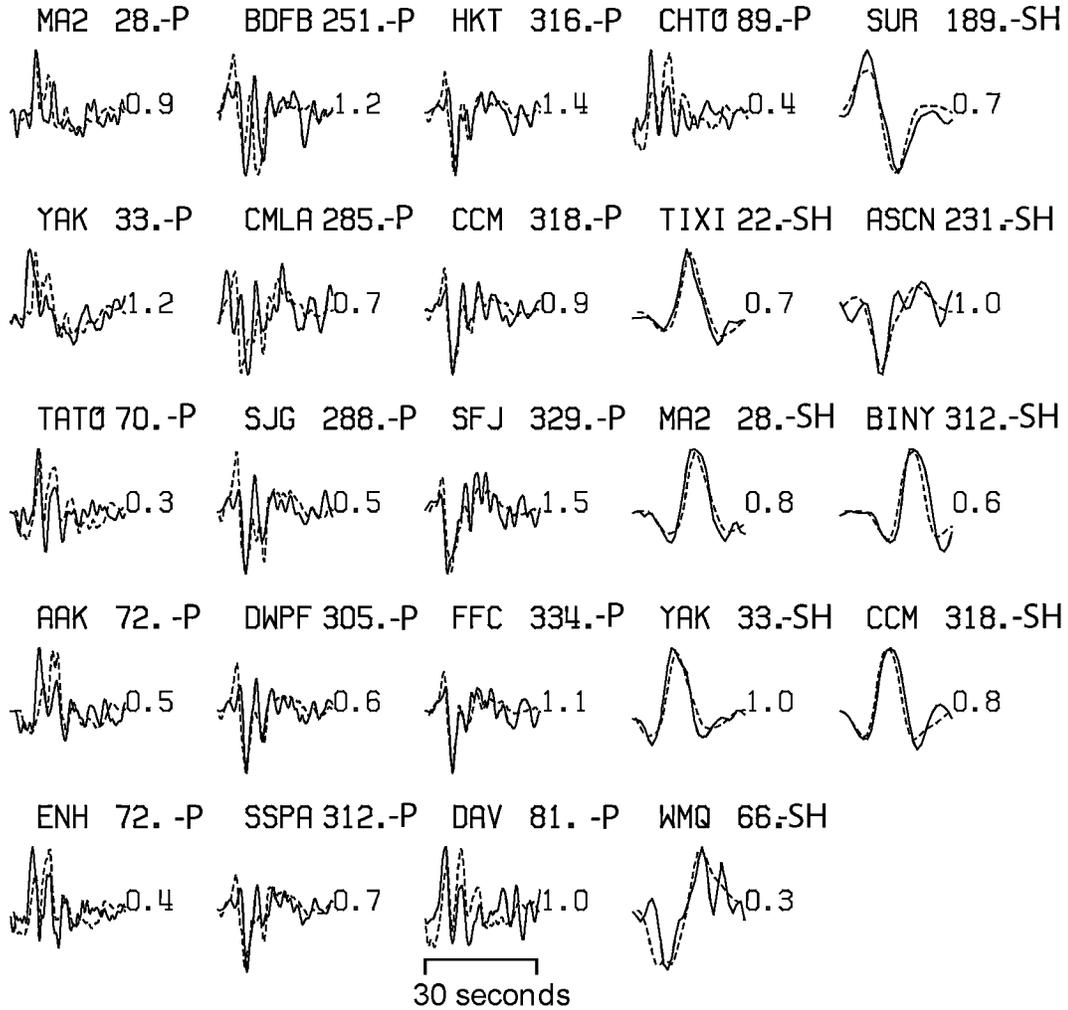## November 12, 1999, Düzce Earthquake

Figure 6. Comparison of the observed waveforms (solid curves) and the synthetic waveforms (dashed curves) calculated for the slip model shown in Fig. 5. Station names and azimuths clockwise from north are given in the top left- and top right-hand of each observed-synthetic waveform pair, respectively. The numbers to the right of each waveform pair indicate synthetic-to-observed amplitude ratios.
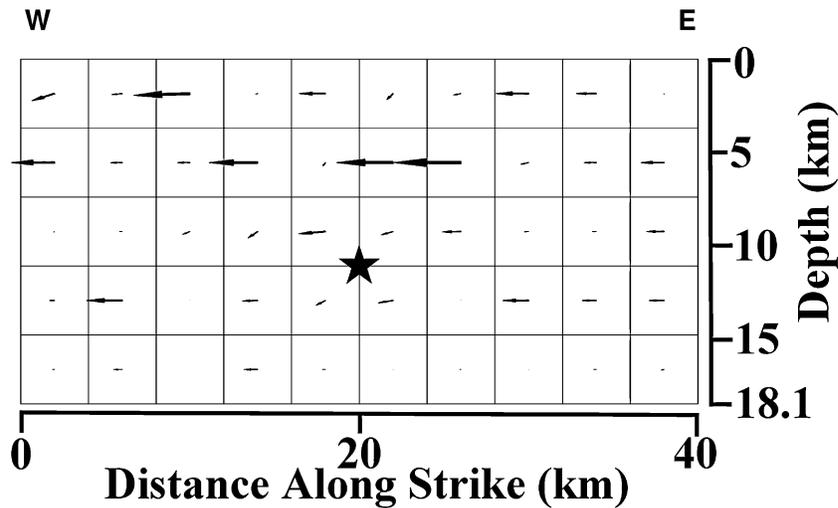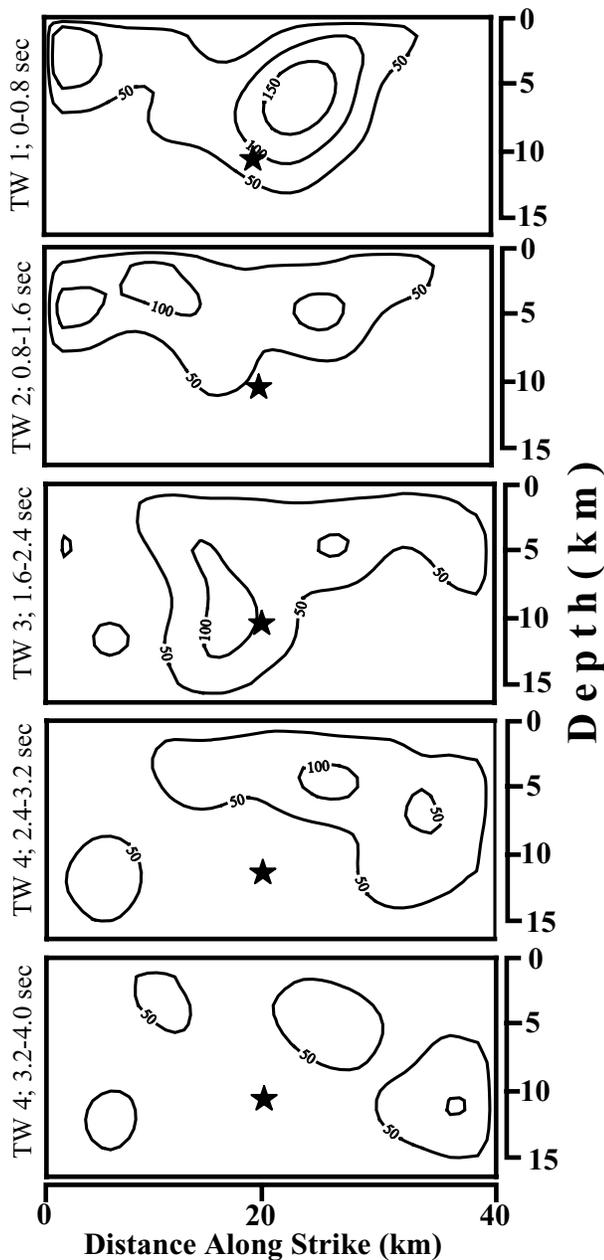

Figure 7. Slip vector for each subfault determined from the inversion, indicating relative motion of the southern fault block and relative slip amplitudes. The solid star shows the hypocentre.

Figure 8. Spatial and temporal slip distribution on the fault plane. Each frame shows the slip distribution within a specified time following the onset of slip at each point, not a snapshot in absolute time. The first frame, for instance, begins at each point immediately after the passage of the fastest (2.5 km s^{-1}) rupture front and shows the distribution of slipping areas for the following 0.8 s. The duration of each frame is shown on its left. The number of frames in which a particular region is slipping is related to the rupture duration in that area, for example, note that the LA is slipping in all five frames, indicating a rupture duration of more than 4 s. In contrast, slip in the bottom left-hand corner initiates at approximately 1.6 s after the initial rupture front passes and continues for approximately 2.4 s. The contour interval is 0.5 m (further explanation of this type of rupture front dependent time-window can be found in Wald & Heaton 1994).

hypocentre, initially breaking the LA and proceeding to break the SA. At the location of LA, slip mainly occurred within the first four time windows with minor slip in the fifth window indicating a rise time of approximately 3 s for the LA. However, significant slip of the

LA occurred in the first time window, requiring no significant delay relative to the maximum rupture velocity selected for the modelling, 2.5 km s^{-1}. The slip in the SA took place within the first two time windows defining a relatively shorter rise time of 1.6 s. Note that almost no slip occurred down dip from the hypocentre within the first two time windows, although there is significant shallow slip. This indicates a decrease in the rupture velocity as the rupture propagates to deeper areas of the fault. Additionally, deeper fault areas show shorter rise times than the shallow areas. For example, the slip just west and down dip of the hypocentre occurred only within the third time windows while the slip across the bottom eastern corner of the fault occurred only within the final time window, both indicating a slip rise time of 0.8 s for the respective fault region. If we do not account for the tiny area of slip in the third time window for the fault region down dip from the SA, the slip in this area is also confined to the final two time windows. Finally, the overall source of the earthquake could be approximated by a slip rise time of 2.5 s, since most of the total slip is consumed within the first three time windows.

Ayhan *et al.* (2001) obtained strike- and dip-slip distributions of the earthquake from inversion of GPS data. Their slip distribution model suggest a large source area east and updip of the hypocentre, with a strike-slip displacement of slightly over 500 cm and a dip-slip displacement of approximately 150 cm. This source exactly overlaps the fault region covered by the LA. The GPS-derived strike-slip motion gradually decreases towards the west and terminates approximately 15 km west of the hypocentre. The GPS-derived dip-slip distribution shows a local decrease at the hypocentral region and then peaks again approximately 150 cm to the west of the hypocentre. However, the teleseismic model suggests dip-slip at the west and updip of the hypocentre mostly less than 100 cm but no dip-slip at the east of the hypocentre (Fig. 5). In another geodetic study, Wright *et al.* (2001) constrained a variable slip model of the earthquake from the inversion of InSAR data. They represented the earthquake rupture with a 45 km long six-segment fault model and retrieved the slip of each segment. The InSAR data required a slip of 2.5 ± 0.6 m for the segment including the hypocentre and 2.9 ± 0.4 and 1.7 ± 0.6 m for the adjacent segments in the west and east, respectively. These three segments approximately cover the rupture area remaining between Eften Lake step over and Kaynaşli town, which approximately corresponds to the LA and its westerly extension (the fault area confined by the 3 m contour in the bottom frame of Fig. 5). The resulting bottom depth, 15.3 ± 1.4 km, is also compatible with the depth extent of the slip in our model. Tibi *et al.* (2001) found a bilateral rupture, which proceeded to the west for 30 km and east for 25 km, from the inversion of the teleseismic broad-band *P* and *SH* waveforms. Easterly propagating rupture released a seismic moment of 3.6×10^{19} N m, which is twice as much as that released by westerly propagation (1.8×10^{19} N m). Their moment release distribution along the strike also resembles that suggested by our slip model.

Barka *et al.* (2000) pointed out that Eften lake step over stopped the rupture of August 17, İzmit earthquake from propagating further east to the Düzce fault. The slip model resulting from this study indicates that the Eften lake step over was not the only reason for the termination of the İzmit rupture but also the LA over the Düzce fault, adjacent to the Eften Lake step over, constituted another impediment to the İzmit rupture. Possibly both impediments caused stress accumulation at the eastern end of the Gölyaka segment that triggered the Düzce earthquake and caused re-rupture of the western part of the Gölyaka segment for 9 km.

COULOMB STRESS CHANGE MODELLING

In this section, we investigate stress transfer from the 1999 İzmit earthquake to the 1999 Düzce fault, and how together with other earlier large earthquakes and tectonic movements since 1943 they change the likelihood of future earthquakes on the branches of the NAFZ. Previous studies (Hubert-Ferrari *et al.* 2000; Pınar *et al.* 2001) only calculated the stress change on optimally oriented slip planes, and did not include the 1999 Düzce earthquake in their calculations. Therefore, we have calculated the Coulomb stress change on previously mapped active faults in the area according to their strike and dip direction and included the Düzce earthquake in our stress calculation using the slip distribution obtained in this study. This approach does not require any regional stress information as required by the more common approach (e.g. Stein *et al.* 1992; King *et al.* 1994) of calculating Coulomb stress change on optimally oriented slip planes. The change in Coulomb stress, $\Delta \sigma_f$, on a target fault is

$$\Delta \sigma_f = \Delta \tau + \mu' \Delta \sigma_n, \tag{1}$$

where $\Delta \tau$ and $\Delta \sigma_n$ are changes in the shear (positive in the fault slip direction) and normal stresses (positive in extension), respectively. μ' is the effective friction coefficient and is thought to include unknown effects of pore-fluid pressure in the crust (Simpson & Reasenberg 1994; Havris 1998). We model faults as rectangular dislocation surfaces embedded in an elastic half-space with elastic constants Young's modulus and Poisson's ratio of 8.0×10^5 bar and 0.25, respectively

We have investigated the stress transfer in two cases; first, only the stress-triggering relationship between the İzmit and Düzce earthquakes and, secondly, the relationship of the Düzce event with all large earthquakes preceding it that occurred in the instrumental period and tectonic loading since 1943. The time interval of this study is limited, by necessity, by the date of the first documented event in the region of interest (i.e. 1943, magnitude 6.3), though previous seismicity also plays a role in the present state of stress. With the exception of Fig. 11 (see below), we calculated the stress change at 6.5 km, half the depth of the average seismogenic layer.

Stress-triggering relation between the 1999 İzmit and 1999 Düzce earthquakes

In order to compute the stress changes owing to the İzmit earthquake on the Düzce event, we must first choose a slip model. We consider four possibilities: Pınar *et al.* (2001), Yagi & Kikuchi (2000), Çakır *et al.* (2002) and Delouis *et al.* (2002). Neither Pınar *et al.* and Yagi & Kikuchi are suitable for our analysis as their simplified models disregard the observed rupture geometry of the earthquake. We therefore employ the most comprehensive slip distribution model (Delouis *et al.* 2002) obtained from a wide variety of data sets including teleseismic, strong motion and geodetic, and calculate Coulomb stress changes due solely to the İzmit mainshock on slip-planes that are oriented parallel to the Düzce fault (i.e. strike=262° and dip=65°); this stress transfer is shown is Fig. 9. Note that when we test our results against the other slip model with the observed complex fault geometry, Çakır *et al.* (2002), we obtain very similar stress changes. The Düzce fault received a stress increase ranging from 0.5 to 12 bar along it at 6.5 km depth. This is an appreciable amount of stress load in a very short time, if one considers that in general stress drops of earthquakes range from 10 to 100 bar (Shearer 1999).

### Stress relation owing to all large earthquakes in the instrumental period

Earlier studies (Deng & Sykes 1997a,b; Stein *et al.* 1997; Nalbant *et al.* 1998; Hubert-Ferrari *et al.* 2000; Nalbant *et al.* 2002) indicated that in order to derive implications for the future seismic hazard for a region, it is extremely important to include previous large earthquake activity and tectonic loading into the stress modelling as far back in time as possible. Without incorporating previous stress history any conclusion based on a single earthquake could be misleading. Nalbant *et al.* (1998) modelled 29 earthquakes ($M_s \geq 6.0$) that occurred at the NW and N Aegean Sea prior to the İzmit earthquake. From their results, the future İzmit rupture was located in an area where stress clearly increased, the Düzce fault, however, was in the area where the stress decreased. In order to improve our understanding of the stress relation between the two earthquakes, we have also included all large earthquakes ($M_s \geq 6.3$) that occurred in the instrumental time period in the modelling and the resulting stress map is shown in Fig. 10. It is interesting to note that in contrast to Fig. 9 only part of the western extension of the Düzce fault has a positive stress load (Figs 10 and 11b), the stress increase on the rest of the fault is not enough to overcome the stress decrease as a result of the preceding earthquakes nearby. Similar relationships between neighbouring faults were observed for some earthquakes in the Aegean Sea (Nalbant *et al.* 1998); faults that had received stress reduction from earlier events were prepared for failure by a nearby earthquake that caused a local stress rise. Also post-seismic deformation during the 3 months after the İzmit event has lead to an additional 0.6 bar increase at the hypocentre of the Düzce earthquake (Hearn *et al.* 2002) that might also help the Düzce fault to move.

The relationship between Coulomb stress change owing to the İzmit rupture and the slip distribution of the Düzce event is shown in Fig. 11(a). Clearly, there is no relation between the two, both the hypocentre and the LA of Düzce are located in regions of only moderate stress increase while the SA spans areas of both positive and negative stress changes.

As shown in Fig. 11(b), the correlation between stress change and slip is even worse when the effects of tectonic loading and previous earthquakes are included. In this case the hypocentre experiences at most a very small positive Coulomb stress increase while the LA lies in a region of negative stress change. In order to test the robustness of these results, they were recomputed using the slip model of Çakır *et al.* (2002). Using their slip inversion, we observed minor changes in the detail of the stress pattern but the overall relationship between stress change and slip was unaltered. As discussed earlier, we do not believe that either the slip model of Pınar *et al.* (2001) or Yagi & Kikuchi (2000) appropriately represent the actual fault geometry of the İzmit event and hence we did consider them here.

As shown in Fig. 11 the hypocentral region was loaded by the İzmit earthquake up to a maximum of 2.5 bar. Once the rupture initiated, it could have been expected to propagate through the highly stressed area to the west. In fact, the rupture can be seen to propagate to the NE of the fault, which experienced greatest slip in a region that had received a stress decrease as a result of the İzmit earthquake. Fig. 11(b) shows that this situation is changed little when other previous earthquakes and the effects of 50 years of tectonic loading are considered.

These results are not consistent with a simple model for the seismic cycle in which stress increases on a fault that then breaks, relieving stress uniformly across its surface. Such a model would have this fault quiescent until the stress again reached the failure strength
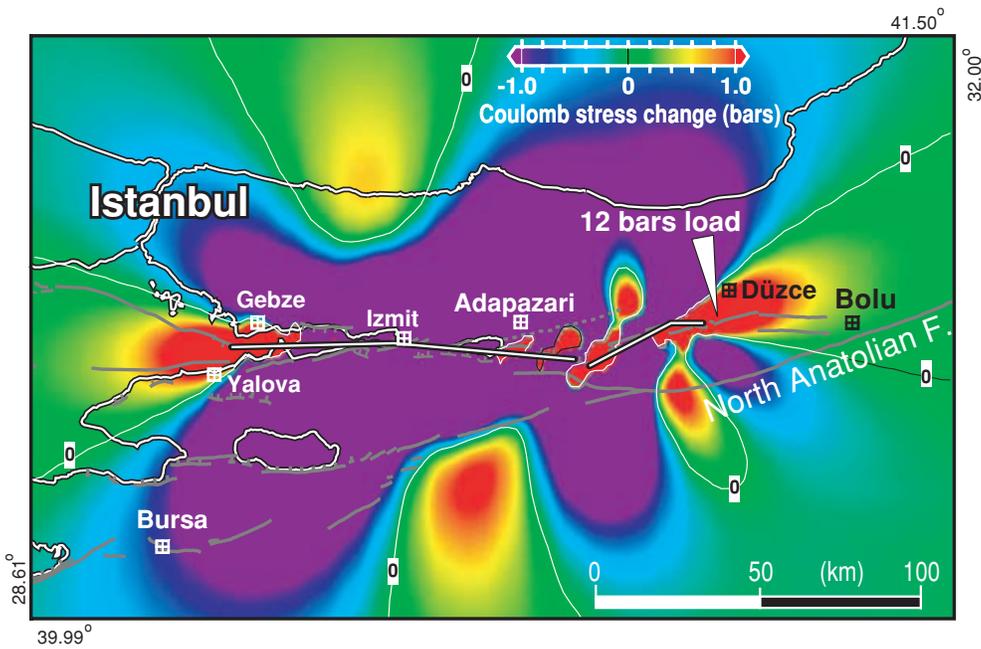
Figure 9. Coulomb stress change caused by the 1999 İzmit earthquake calculated on slip-planes that are parallel to the Düzce fault. The stress is sampled at 6.5 km depth. The slip model of Delouis *et al.* (2002) is used. The Düzce fault, activated approximately 3 months later, has received stress increases ranging from 0.5 to 12 bar. Although the faults beneath the Sea of Marmara also experienced considerable stress increase, there was an earthquake in 1963 close to the town of Yalova; its stress shadow possibly persists and arrested the continuation of the İzmit rupture further west and delayed any future earthquake (Hubert-Ferrari *et al.* 2000). White lines enclosed with black indicate coastlines.
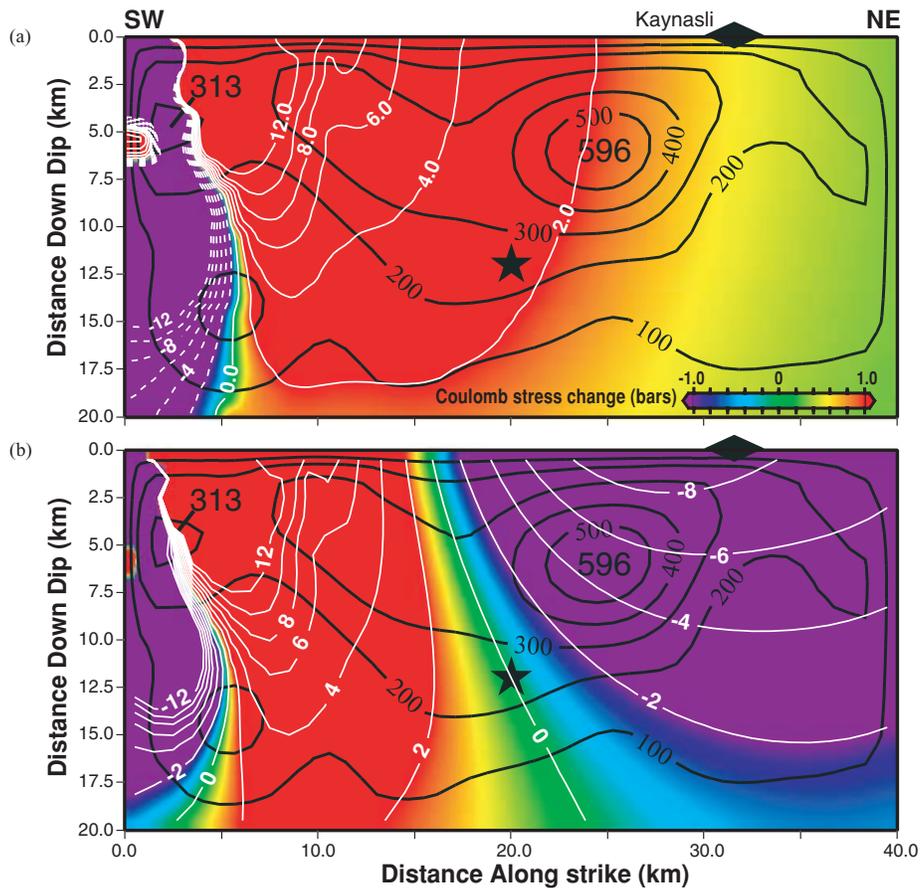
Figure 11. (a) Coulomb stress change as a result of the İzmit earthquake on the cross-section of the Düzce fault, and a comparison between the stress load and the calculated total slip distribution. Slip contours are in centimetres. (b) Comparison between the stress load as a result of all large earthquakes and tectonic loading since 1943 and the calculated total slip distribution.
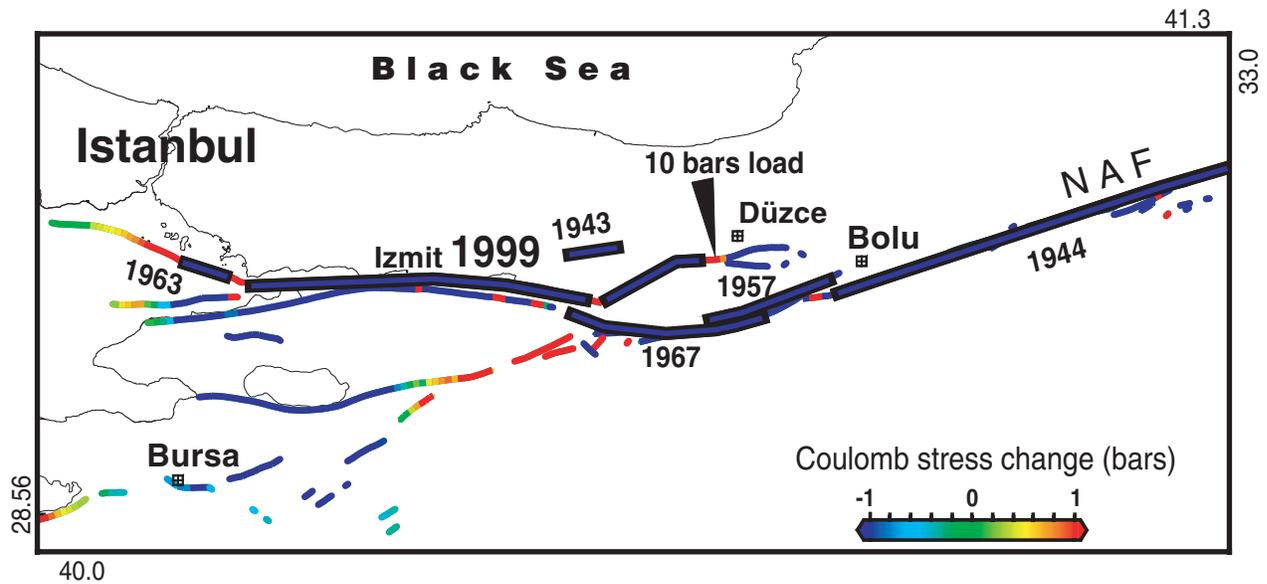
Figure 10. Stress change before the 1999 Düzce earthquake as a result of large earthquakes ($M_s \geq 6.3$) since 1943 in the area. Faults that ruptured are outlined by black rectangles. Earthquake occurrence times are also shown. The stress is calculated at 6.5 km depth. Note that a portion of the Düzce fault remains highly loaded.
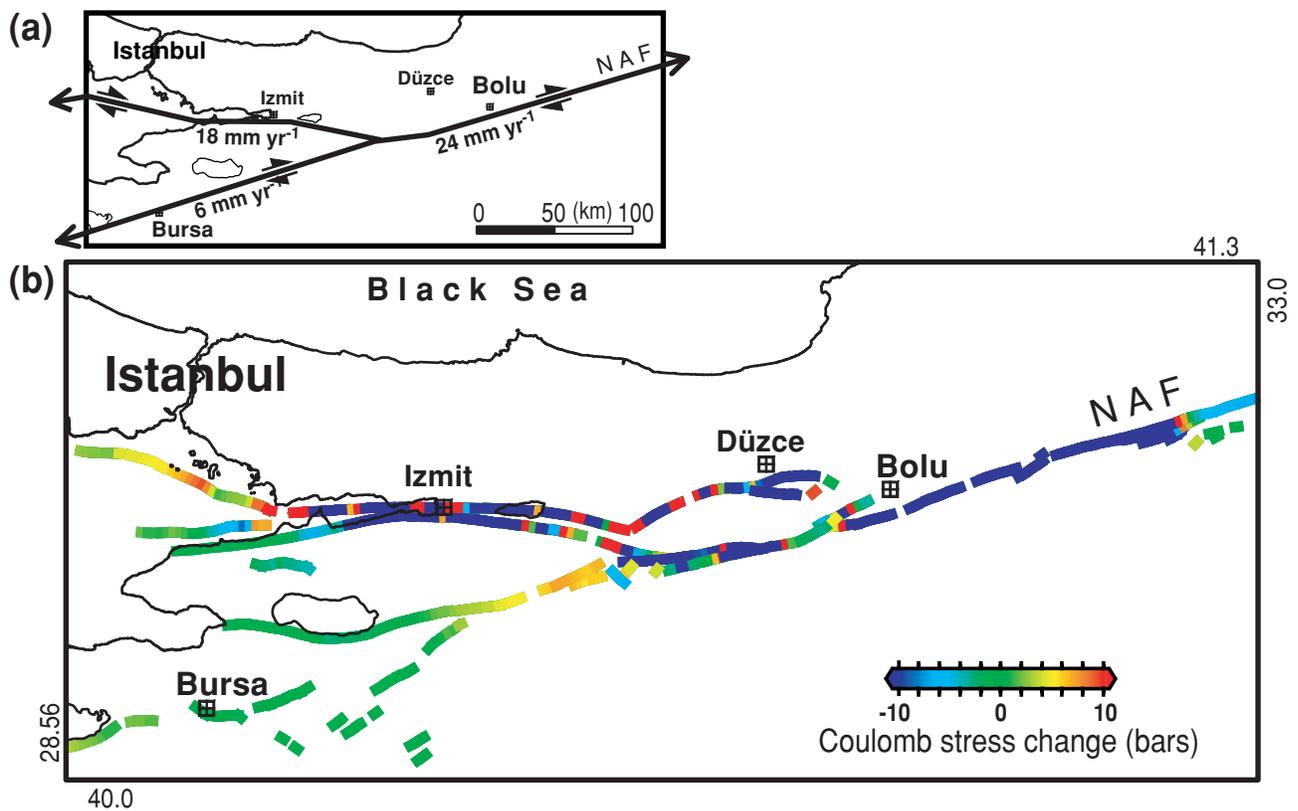
Figure 12. (a) The geometry of the long-term tectonic loading model. The simulation was made by introducing dislocation surfaces beneath the seismogenic zone and moving them at the rate calculated by GPS measurements (Straub 1996; McClusky *et al.* 2000). (b) Coulomb stress map arising from all the large earthquakes ($M_s \geq 6.3$) that occurred in the instrumental period and the tectonic movements since 1943.

when it would again fail in an event that is characteristic of the fault in question. Here we see a distinct lack of correlation between stress and slip, which indicates a more complex relationship between stress, strength and event history on the plane. In this view, an earth-quake is a response to an interplay between tectonic loading, stress relaxation arising from small events on the fault plane, dynamic stress concentrations at the rupture front and, vitally, an extremely heterogeneous strength distribution (see Steacy & McCloskey 1998,

for a discussion). It is clear that this lack of correlation over the area of the rupture has no bearing on the validity of the Coulomb stress hypothesis in explaining the Düzce earthquake. For the event to be consistent with Coulomb triggering we need only observe a Coulomb stress increase at the hypocentre. This is clearly the case here.

Fig. 12 shows the Coulomb stress change as a result of large earthquakes and tectonic movements since 1943. The northern branch of the NAF in the Marmara Sea (Princess Island fault) has been loaded by both the 1999 İzmit earthquake and tectonically from 5 to 10 bar. Faults beneath the Sea of Marmara close to the town of Yalova have received stress increases of up to 6.5 bar locally. When tectonic loading is accounted for the area the stress level reaches 10.5 bar (Fig. 12b), making the area a likely place for a future damaging earthquake. The stress decrease caused by the 1963 earthquake is almost erased. On the other hand, the faults close to the city of Yalova on the land are loaded up to 1.2 bar.

The Düzce earthquake loads the NE portion of the 1957 rupture up to 5.2 bar locally while causing stress decreases along the majority of the 1957 and 1967 faults by as much as -6.8 bar. The SW end of the 1944 rupture receives a stress reduction of up to -1.5 bar, although the rest of it receives an approximately 0.1 bar increase. Most of the stress loading is caused by the accumulated secular stress arising from tectonic movements. The main branch of the NAFZ receives 0.16 bar yr^{-1} while northern and southern branches further west receive 0.125 and 0.07 bar yr^{-1}, respectively. The stress level on the 1944 segment of the NAFZ is approximately -25 bar and with a rate of 0.16 bar yr^{-1} as a result of tectonic loading, it would take 157 yr to recover from the stress shadow, and possibly another 157 yr to reach the stress level prior to the 1944 earthquake. However, the occurrence of any neighbouring earthquake could easily change this time span.

CONCLUSIONS

Finite-fault inversion of teleseismic *P* and *SH* waveforms of the 1999 November 12, Düzce earthquake are performed to obtain a coseismic slip model of the earthquake. The teleseismically derived slip model suggests that the earthquake involves the failure of two major asperities. One asperity is located to the east, updip of the hypocentre with a peak slip of 5.96 m, while the other asperity is located near the top corner of the fault in the west with a peak slip of 3.13 m. The rupture is bilateral and mostly above the hypocentral depth. The total seismic moment is 5.5×10^{19} N m, most of which is released by the easterly propagating rupture. In addition to the Eften lake step over located between the Gölyaka fault segment and the Düzce fault, the large asperity also appears to have contributed to rupture termination of the 1999 August 17, İzmit event. The coseismic slip distribution model and the observed surface slip distribution correlate well.

Static stress modelling of earthquakes from 1943 suggests that the Düzce rupture was triggered by the İzmit event, which changed the stress state at the hypocentral location from negative to positive. Interestingly, the calculated slip distribution in the Düzce earthquake does not correspond with with the mapped stress change anomalies on the fault surface; for example the greatest slip occurred in a region that experienced only a modest stress increase from the İzmit event and a net stress decrease when all events since 1943 were included in the modelling. This is potentially a very interesting result and work is underway to examine whether this lack of correlation between stress and slip is observed for other earthquake pairs.

This observation does not invalidate the hypothesis that Coulomb stress changes can trigger subsequent events. Much of the rupture plane of the Düzce earthquake experienced a positive Coulomb stress change, as did the hypocentre, and this is clearly consistent with Coulomb triggering. The lack of correlation between stress change and slip does, however, support the view that the size of an earthquake is controlled by rupture propagation (e.g. Abercrombie & Mori 1994) and that small earthquakes are important in preparing a fault zone for failure (Steacy & McCloskey 1998). In this view it was the dynamic stress perturbations ahead of the propagating rupture and the small-scale (and unmodelled) pre-existing stress perturbations on the fault plane that enabled the large slip in a region of Coulomb stress decrease while the positive Coulomb perturbation acted as a trigger for the initial rupture.

The combined static stress modelling including both co-seismic (all large events since 1943) and secular loading shows that the northern branch of the North Anatolian fault zone, beneath the Sea of Marmara towards the city of İstanbul, is the most highly loaded segment of the fault zone and might, therefore, be expected to produce the next large, damaging earthquake.

REFERENCES

Abercrombie, R. & Mori, J., 1994. Local observations of the onset of a large earthquake: 28 June 1992 Landers, California, *Bull. seism. Soc. Am.,* **84,** 725–734.

Aki, K. & Richards, P.G., 1980. *Quantative Seismology: Theory and Methods,* Freeman, San Francisco, CA.

Akyüz, H.S., Hartleb, R., Barka, A., Altunel, E., Sunal, G., Meyer, B. & Armijo, R., 2002. Surface rupture and slip distribution of the 12 November 1999 Düzce earthquake (*M* 7.1), North Anatolian Fault, Bolu, Turkey, *Bull. seism. Soc. Am.,* **92,** 61–66.

Ayhan, M.E., Bürgmann, R., McClusky, S., Lenk, O., Aktug, B., Herece, E. & Reilinger, R.E., 2001. Kinematics of the $M_w = 7.2$, 12 November 1999, Düzce, Turkey earthquake, *Geophys. Res. Lett.,* **28,** 367–370.

Barka, A., 1996. Slip distribution along the North Anatolian Fault associated with the large earthquakes of the period 1939 to 1967, *Bull. seism. Soc. Am.,* **86,** 1238–1254.

Barka, A., 1999. The 17 August 1999 İzmit earthquake, *Science,* **285,** 1858–1859.

Barka, A.A. & Kandisky-Cade, K., 1988. Strike-slip fault geometry geometry in Turkey and its influence on earthquake activity, *Tectonics,* **7,** 663–684.

Barka, A., Altunel, E., Akyüz, S., Sunal, G., Hartleb, R., Uslu, O.B. & Toroman, E., 1999. The November 12 Düzce earthquake, *Bilim Teknik,* **385,** 40–42 (in Turkish).

Barka, A., Kozaci, O., Akyüz, S. & Altunel, E., eds, 2000. *The 1999 İzmit and Düzce Earthquakes: Preliminary Results.* İstanbul Technical University, İstanbul.

Bürgmann, R. *et al.*, 2002. Deformation during the 12 November 1999 Düzce, Turkey, earthquake from GPS and InSAR data, *Bull. seism. Soc. Am.,* **92,** 161–171.

Çakır, Z., De Chabalier, J.B., Armijo, R., Meyer, B. & Peltzer G., 2002. Fault rupture geometry, kinematics and slip distribution of the 1999 Izmit earthquake (Turkey), determined from SAR interferometry and tectonic field observations, *Geophys. J. Int.,* to be submitted

Delouis, B., Giardini, D., Lundgren, P. & Salichon, J., 2002. Joint inversion of InSAR, teleseismic and strong motion data for the spatial and temporal distribution of earthquake slip: application to the 1999 İzmit mainshock, *Bull. seism. Soc. Am.,* **92,** 278–299.

Deng, J. & Sykes, L.R., 1997a. Evolution of the stress field in southern California and triggering of moderate-size earthquakes: a 200-year perspective, *J. geophys. Res.,* **102,** 9859–9886.

Deng, J. & Sykes, L.R., 1997b. Stress evolution in southern California and triggering of moderate-, small-, and micro-size earthquakes, *J. geophys. Res.,* **102,** 24 441–24 435.

Hall, J.F., Heaton, T.H., Halling, M.W. & Wald, D.J., 1995. Near-source ground motion and its effect on flexible buildings, *Earthquake Spectra,* **11,** 569–605.

Harris, R.A., 1998. Introduction to special section: stress triggers, stress shadows, and implications for seismic hazard, *J. geophys. Res.,* **103,** 24 347–24 358.

Hartzell, S.H., 1989. Comparison of waveform inversion results for the rupture history of finite fault; application to the 1986 North Palm Springs, California, earthquake, *J. geophys. Res.,* **94,** 7515–7534.

Hartzell, S.H. & Heaton, T.H., 1983. Inversion of strong-ground motion and teleseismic wave form data for the fault rupture history of the 1979 Imperial Valley, California, earthquake, *Bull. seism. Soc. Am.,* **73,** 1553–1583.

Hartzell, S. & Langer, C., 1993. Importance of model parameterisation in finite fault inversions: application to the 1974 M_w = 8.0 Peru Earthquake, *J. geophys. Res.,* **98,** 22 123–22 134.

Hartzell, S.H., Harmsen, S., Frankel, A. & Larsen, S., 1999. Calculation of broadband time histories of ground motion: comparison of methods and validation using strong-ground motion from the 1994 Northridge earthquake, *Bull. seism. Soc. Am.,* **89,** 1484–1504.

Hearn, E.H., Bürgmann, R. & Reilinger, R.E., 2002. Dynamics of İzmit earthquake postseismic deformation and loading of the Düzce earthquakes hypocenter, *Bull. seism. Soc. Am.*, **92,** 172–193.

Honkura, Y. *et al.*, 2000. Preliminary results of multidisciplinary observations before, during and after the Kocaeli (Izmit) earthquake in the western part of the North Anatolian Fault Zone, *Earth, Planets Space,* **52,** 293–298.

Hubert-Ferrari, A., Barka, A., Jacques, E., Nalbant, S.S., Meyer, B., Armijo, R., Topponnier, P. & King, G.C.P., 2000. Seismic hazard in the Marmara sea region following the 17 August 1999 İzmit earthquake, *Nature,* **404,** 269–273.

Jackson, J. & McKenzie, D.P., 1984. Active tectonics of the Alpine–Himalayan belt between western Turkey and Pakistan, *Geophys. J. R. astr. Soc.,* **77,** 185–264.

Kenar, Ö. & Toksöz, N., 1989. Dispersion and attenuation properties of surface waves in Anatolia, *Jeofizik,* **3,** 92–106(in Turkish).

King, G.C.P., Stein, R.S. & Lin, J., 1994. Static stress changes and triggering of earthquakes, *Bull. seism. Soc. Am.,* **84,** 935–953.

Langer, C.J. & Hartzell, S., 1996. Rupture distribution of the 1977 western Argentina earthquake, *Phys. Earth planet. Inter.,* **94,** 121–132.

Langston, C.A. & Helmberger, D.V., 1975. A procedure for modelling dislocation sources, *Geophys. J. R. astr. Soc.,* **42,** 117–130.

Lawson C.L. & Hanson, R.J., 1974. *Solving Least Square Problem,* Prentice-Hall. Englewood Cliffs, NJ.

McClusky, S. *et al.*, 2000. GPS constraints on plate kinematics and dynamics in the Eastern Mediterranean and Caucasus, *J. geophys. Res.,* **105,** 5695–5719.

McKenzie, D.P., 1972. Active tectonics of the Mediterranean region, *Geophys. J. R. astr. Soc.,* **30,** 109–185.

Mendoza, C., 1995. Finite-fault analysis of the 1979 March 14 Petetlan, Mexico, earthquake using teleseismic, *P* wave forms. *Geophys. J. Int.,* **121,** 675–683.

Mendoza, C., Hartzell, S. & Monfret, T., 1994. Wide-band analysis of the 3 March 1985 central Chile earthquake: overall source process and rupture history, *Bull. seism. Soc. Am.,* **84,** 269–283.

Nalbant, S.S., Hubert, A. & King, G.C.P., 1998. Stress coupling between earthquakes in northwest Turkey and the north Aegean Sea, *J. geophys. Res.,* **103,** 24 469–24 486.

Nalbant, S.S., McCloskey, J., Steacy, S. & Barka, A.A., 2002. Stress accumulation and increased seismic risk in Eastern Turkey, *Earth planet. Sci. Lett.,* **195,** 291–298.

Örgülü, G. & Aktar, M., 2001. Regional moment tensor inversion for strong aftershocks of the August 17, 1999 İzmit earthquake (M_w = 7.4), *Geophys. Res. Lett.,* **28,** 371–374.

Parsons, T., Shinji, T., Stein, R.S., Barka, A. & Dietrich, J.H., 2000. Heightened odds of large earthquakes near İstanbul: an interaction-based probability calculation, *Science,* **288,** 661–665.

Pınar, A., Kikuchi, M. & Honkura, Y., 1994. Rupture process of the 1992 Erzincan earthquake and its implication for the seismotectonics in eastern Turkey, *Geophys. Res. Lett.,* **21,** 1971–1974.

Pınar, A., Kikuchi, M. & Honkura, Y., 1996. A rupture model of the 1967 Mudurnu Valley earthquake and its implication for seismotectonics of the western part of the North Anatolian fault Zone, *Geophys. Res. Lett.,* **23,** 29–32.

Pınar, A., Honkura, Y. & Kuge, K., 2001. Seismic activity triggered by the 1999 İzmit earthquake and its implications for the assessment of future seismic risk, *Geophys. J. Int.,* **146,** F1–F7.

Seber, D., Vallve, M., Sandvol, E., Steer, D. & Barazangi, M., 1997. Geographic Information Systems (GIS) in earth sciences: an application to the Middle East region, *GSA Today,* **7,** 1–6.

Shearer, P.M., 1999. *Introduction to Seismology,* Cambridge University Press, Cambridge.

Simpson, R.W. & Reasenberg, P.A., 1994. Earthquake-induced static stress changes on central California faults, in the Loma Prieta, California earthquake of October 17, 1989—tectonic processes and models, ed. Simpson R.W., *US Geological Survey Prof.* Paper 1550–F.

Steacy, S.J. & McCloskey, J., 1998. What controls an earthquake's size? Results from a heterogeneous cellular automaton, *Geophys. J. Int.,* **133,** f11–f14.

Stein, R.S., King, G.C.P. & Lin, J., 1992. Change in failure stress on the southern San Andreas fault system caused by the 1992 magnitude = 7.4 Landers earthquake, *Science,* **258,** 1328–1332.

Stein, R., Barka, A. & Dietrich, J.H., 1997. Progressive failure on the North Anatolian fault since 1939 by earthquake stress triggering, *Geophys. J. Int.,* **128,** 594–604.

Straub, C., 1996. Recent crustal deformation and strain accumulation in the Marmara Sea region, N.W. Anatolia, inferred from GPS measurements, *PhD thesis,* Swiss Federal Institute of Technology, Zurich.

Tibi, R. *et al.*, 2001. Rupture processes of the 1999 August 17 Izmit and November 12 Düzce (Turkey) earthquakes, *Geophys. J. Int.,* **144,** F1–F7.

Toksöz, M.N., Shakal, A.F. & Micheal, A.J., 1979. Space–time migration of earthquakes along the North Anatolian Fault Zone and seismic gap, *Pure appl. Geophys.,* **117,** 1258–1270.

Toksöz, M.N., Reilinger, R.E., Doll, C.G., Barka, A.A. & Yalçın, N., 1999. İzmit (Turkey) earthquake of 17 August 1999: first report, *Seism. Res. Lett.,* **70,** 669–679.

Wald, D.J. & Heaton, T.H., 1994. Spatial and temporal distribution of slip for the 1992 Landers, California, earthquake, *Bull. seism. Soc. Am.,* **84,** 668–691.

Wald, D.J., Heaton, T.H. & Helmberger, D.V., 1991. Rupture model of the 1989 Loma Prieta earthquake from the inversion of strong motion and broadband teleseismic data, *Bull. seism. Soc. Am.,* **81,** 1540–1572.

Wright, T., Fielding, E. & Parsons, B., 2001. Triggered slip: observations of the 17 August 1999 Izmit (Turkey) earthquake using radar interferometry, *Geophys. Res. Lett.,* **28,** 1079–1082.

Yagi, Y. & Kikuchi, M., 2000. Source rupture process of the Kocaeli, Turkey, earthquake of August 17, 1999, obtained by joint inversion of near-field and teleseismic data, *Geophys. Res. Lett.,* **27,** 1969–1972.